Computational and Structural Biotechnology Journal 18 (2020) 2217–2227

COMPUTATIONAL AND STRUCTURAL BIOTECHNOLOGY JOURNAL

journal homepage: www.elsevier.com/locate/csbj

Predicting combinations of immunomodulators to enhance dendritic cell-based vaccination based on a hybrid experimental and computational platform

Rita Ahmed [a,b,1], Isaac Crespo [a,b,c,1], Sandra Tuyaerts [d], Amel Bekkar [e], Michele Graciotti [a,b], Ioannis Xenarios [e], Lana E. Kandalaft [a,b,*]

[a] Department of Oncology, University Hospital of Lausanne, Lausanne, Switzerland
[b] Ludwig Institute for Cancer Research, University of Lausanne (UNIL), Lausanne, Switzerland
[c] Vital-IT group, SIB Swiss Institute of Bioinformatics, University of Lausanne (UNIL), Lausanne, Switzerland
[d] Department of Oncology, Leuven Cancer Institute (LKI), University of Leuven (KU Leuven), Leuven, Belgium
[e] Center for Integrative Genomics, University of Lausanne (UNIL), Lausanne, Switzerland

ARTICLE INFO

Article history:
Received 13 May 2020
Received in revised form 28 July 2020
Accepted 1 August 2020
Available online 8 August 2020

Keywords:
Dendritic cells
Vaccines
Cancer
Immunotherapy
Algorithm
Hybrid platform
Prediction

ABSTRACT

Dendritic cell (DC)-based vaccines have been largely used in the adjuvant setting for the treatment of cancer, however, despite their proven safety, clinical outcomes still remain modest. In order to improve their efficacy, DC-based vaccines are often combined with one or multiple immunomodulatory agents. However, the selection of the most promising combinations is hampered by the plethora of agents available and the unknown interplay between these different agents. To address this point, we developed a hybrid experimental and computational platform to predict the effects and immunogenicity of dual combinations of stimuli once combined with DC vaccination, based on the experimental data of a variety of assays to monitor different aspects of the immune response after a single stimulus. To assess the stimuli behavior when used as single agents, we first developed an *in vitro* co-culture system of T cell priming using monocyte-derived DCs loaded with whole tumor lysate to prime autologous peripheral blood mononuclear cells in the presence of the chosen stimuli, as single adjuvants, and characterized the elicited response assessing 18 different phenotypic and functional traits important for an efficient anti-cancer response. We then developed and applied a prediction algorithm, generating a ranking for all possible dual combinations of the different single stimuli considered here. The ranking generated by the prediction tool was then validated with experimental data showing a strong correlation with the predicted scores, confirming that the top ranked conditions globally significantly outperformed the worst conditions. Thus, the method developed here constitutes an innovative tool for the selection of the best immunomodulatory agents to implement in future DC-based vaccines.

1. Introduction

Cancer is a second leading cause of death worldwide accounting for 9.6 million of deaths in 2018 [1]. The increasing number of new cancer cases every year stimulates the research of novel treatments to improve the prognosis of cancer patients. Immunotherapy emerged as an established pillar of cancer treatment inducing a durable response in multiple solid and hematologic malignancies. Dendritic cell (DC)-based vaccines are a promising arm of cancer immunotherapy boosting the patient's own immune response against their tumors. As professional antigen-presenting cells (APCs), DCs capture and present pathogen-associated antigens to T cells, resulting in priming and activation of an effector T cell response [2–4]. Encouraging preclinical and clinical studies led to the approval of the first cellular-based cancer vaccine Sipuleucel-T, used against metastatic castration-resistant prostate cancer by the Food and Drug Administration. The vaccine is well tolerated and demonstrated a significant increase of overall survival by 4.1 months [5]. Despite the growing number of DC-based vaccine clinical studies, the clinical response remains modest with a 10–20% objective response rate, urging the need to

* Corresponding author at: Department of Oncology, University Hospital of Lausanne, Lausanne 1011, Switzerland.
E-mail address: Lana.Kandalaft@chuv.ch (L.E. Kandalaft).
[1] These authors contributed equally.

https://doi.org/10.1016/j.csbj.2020.08.001
2001-0370/

develop new avenues to harness and release the true immunological power of DCs [6]. The lack of strong efficacy can be partially attributed to tumor-mediated immunosuppression mechanisms orchestrated by tumor cells [7,8]. The induction of the immune response depends on three major signals: (1) the antigen-specific interaction between Major Histocompatibility Complex (MHC) molecules present at the DC cell surface with the cognate T cell receptor, (2) the interaction between DC co-stimulatory molecules (e.g. CD83) and their respective ligands at the T cell surface (e.g. CD28) and (3) the secretion of cytokines to polarize the immune response towards a T helper 1 (Th1) phenotype. Cancer cells orchestrate a plethora of factors and signals in the tumor microenvironment that impair the above-mentioned three signals essential for a robust and effective T cell response. These mechanisms include: i) impaired DC maturation and antigen presentation [9,10], (ii) defective trafficking to the draining lymph nodes where T cell priming occurs [11], (iii) diminished surface expression of co-stimulatory molecules [12], (iv) induction of an immunoregulatory cytokine production profile [13] and (v) surface expression of immunosuppressive molecules (e.g.PD-L1, IDO1) [14]. In particular, IL-12, IL-18, IL-21, IL-15, IFNγ, CD40L, 4-1BBL, anti-CTLA-4, and anti-PD-L1 commercially available immunomodulators were chosen at this stage as the most commonly used adjuvants in DC vaccination studies. The selected modulators target the immune system at different levels: i) inducing either an enhanced co-stimulatory signaling (CD40L, 4-1BBL), ii) promoting a Th1 polarized response (IL-12, IL-18, IL-21, IL-15 and IFNγ) or removing inhibitory signals that dampen immune responses (checkpoint blockade inhibition by anti-PD-L1 and anti-CTLA-4). Moreover, IL-12 and IL-15 are involved in the engagement of Natural Killer (NK) cells in the immune response. Table 1 summarizes their main immunomodulatory functions. IL-12 is a central cytokine in the immune response composed of two covalently linked glycosylated chains. It is mainly produced by macrophages, monocytes and mature DCs in response of bacterial products. IL-12 is necessary for the optimal generation of Th1 $CD4^+$ T cells as the balance Th1/Th2 is determined at the initiation of the response [15]. IL-12 enhances NK cells and Cytotoxic T lymphocyte (CTL) functionality influences through an increased production of IFNγ which also contribute to the development of a Th1 response [16]. IL-12 also provides DCs with activation signals required for an efficient priming of T cells [17].

IL-18 is a strong driver of IFNγ production in both NK and T cells, and can act together with IL-12 in priming IFNγ producing Th1 response [18]. A murine study showed that IL-18 transfected DCs were able to expand the repertoire of anti-tumor Th1 type immunity in association of an enhanced therapeutic effect [19]. IL-21 is mainly produced by Th17 cells and plays a central role in the differentiation and proliferation of B and T cells [20]. In a study led by the group of Prof Hooijberg and colleagues, IL-21 transfected into DCs significantly enhanced the priming efficiency of DCs and enhanced the generation of tumor specific $CD8^+$ T cells *in vitro* [21]. IL-15 has a potent stimulatory effect on both innate and adaptive response: The group of Kris Thielemans has demonstrated that, by transfecting IL-15 in DCs, there is an increased phenotypic NK cell activation and NK cell mediated killing of tumor cells [22]. In another study led by the same group they were able to show a superior expansion of tumor specific $CD8^+$ T cells [23]. IFNγ is an important Th1 cytokine, produced in the early stage of the immune response by NK cells and in later stage by T cells. IFNγ also contributes to DC differentiation and maturation [24]. An increased production of IFNγ leads to the elimination of cancer cells. Resistance to immunotherapy is partially attributed to defects in IFNγ signaling [25]. CD40L is an important co-stimulatory molecule preferentially expressed on activated $CD4^+$ T cells, CD40L binds to its cognate molecule CD40 is expressed on APCs including DCs. The interaction CD40-CD40L is involved in the activation of DCs with upregulation of co-stimulatory molecules and production of Th1 polarizing cytokines [26]. 4-1BBL is expressed predominantly on APCs including DCs whereas its cognate receptor 4-1BB is expressed on activated $CD4^+$ and $CD8^+$ T cells. The receptor-ligand interaction amplifies the $CD4^+$ and $CD8^+$ T cells mediated immune response and prolongs the survival of $CD8^+$ cells by prevention of activation-induced apoptosis [27,28]. CTLA-4 is an inhibitory molecule expressed on activated or exhausted $CD4^+$ and $CD8^+$ T cells which bind to the receptor CD80/CD86 with higher affinity than its normal counterpart CD28. By limiting the interaction with CD28, the interaction with CTLA-4 increases the activation threshold of T cells [29]. PD-L1 is an inhibitory molecule expressed at the surface of DCs, it binds to its receptor expressed on activated or exhausted $CD4^+$ and $CD8^+$ T cells. Mature DC express high level of PD-L1 which dampens the efficacy of DC vaccine. Silencing PD-L1 molecule along with IL-15 transpresentation resulted a superior T cell proliferation and IFNγ and TNFα production and promote antigen-specific T cell responses [23].

In addition, so far, most of the studies focused on the role of T cells as they are considered the main players of the anti-cancer response. However, recognition and elimination of cancer by T cells is only one aspect of the anti-tumor response. The cooperation between different components of the immune system is essential for an effective anti-cancer immune response to occur [30]. DC vaccines have the potential to activate other cellular components of the immune system in addition to T cells [31]; moreover the presence of immunosuppressive cells (e.g. regulatory T cells (Treg), myeloid derived suppressor cells) or molecules (e.g. IL-10, TGFβ) in the tumor microenvironment can further hamper the induced immune response [32]. Thus, in order to improve the clinical outcomes of DC vaccine therapy, the global complexity of an immune response must be carefully considered and assessed.

One way to potentially boost DC vaccine efficacy is to counteract the tumor immunosuppressive mechanisms by combining the vaccine with immunomodulatory agents or adjuvants targeting these signaling pathways [33]. These agents can be either directly injected systemically or combined with transfection methods (lipofection, viral transfection or electroporation) into DCs for a more localized and sustained release. Many successful studies demonstrate the feasibility of this approach, with encouraging results in cancer patients [34,35]. Nonetheless, with the plethora of immunomodulatory cues currently available and the mostly unknown effects and interactions of their combinations it is currently difficult if not impossible to select the best combination of stimuli to combine with DC vaccination, without a cumbersome screening and parallel comparison of all possible combinations. To ease this process and the identification of the best possible combinations to use in the context of DC-based vaccines, we have developed a hybrid experimental and computational framework to predict the effect of dual combinations based on the experimental data of single stimuli with enough accuracy to be able to rank and compare them, so that the best and worst candidates can be further investigated and discarded, respectively.

2. Materials and methods

2.1. Hypochlorous acid (HOCl) oxidation of whole tumor cells and preparation of tumor lysate

The melanoma cell line Me290, expressing the MART-1 surface epitope was kindly provided by Prof Daniel Speiser (University of Lausanne, Switzerland). Tumor cells were cultured at 37 °C, 5% CO_2 in Roswell Park Memorial Institute medium (RPMI, Thermo Fisher Scientific, Massachusetts, USA) supplemented with 10% fetal

Table 1
List of the selected immunomodulators with their main function and their respective involvement in the different aspects of the immune response. A positive action of the stimuli on the feature is marked with a "+".

Stimuli	Main Function	Th1 response	$CD4^+$ help	CTL cytotoxicity	NK cell cytotoxicity	T cell proliferation	Memory phenotype	References
IL-12	Co-stimulation	+	+	+	+		+	[23,24]
IL-18	Co-stimulation	+		+		+		[25,26]
IL-21	Co-stimulation			+		+	+	[27,28]
IL-15	T cell proliferation/ memory			+	+	+	+	[29,30]
IFNγ	T cell cytokine secretion	+	+					[31]
CD40L	Co-stimulation		+					[32–34]
4-1BBL	Co-stimulation			+		+	+	[35]
Anti-CTLA-4	Inhibition	+					+	[36]
Anti-PD-L1	Inhibition	+		+		+		[37,38]

bovine serum (FBS, Gibco by Life Technologies, Grand Island, NY, USA) and 5% penicillin–streptomycin (Gibco by Life Technologies, Grand Island, NY, USA) and routinely assessed for Mycoplasma contamination. Tumor lysates were prepared as previously described [36]. Briefly, tumor cells were resuspended at a cell density of 1×10^6 cells/mL in PBS (Gibco by Life Technologies, Grand Island, NY, USA), in the presence of 60 μM of HOCl (Sigma-Aldrich Corp., Darmstadt, Germany). The tumor cell suspension was incubated for 1 h at 37 °C, 5% CO_2 with gentle agitation after every 30 min. After that, tumor cells were harvested, washed twice with PBS and resuspended at 1×10^7 cells/mL in RPMI, followed by six rounds of freeze and thaw. Tumor lysate was stored at −80 °C until further use.

2.2. DC generation

Monocyte-derived dendritic cells (moDCs) were generated from monocytes isolated from fresh peripheral blood mononuclear cells (PBMCs) of human healthy donors collected at the local Blood Transfusion Center Lausanne, Switzerland, under Institutional Review Board approval (Ethics Committee, University Hospital of Lausanne-CHUV). Written informed consent was obtained from all healthy subjects, in accordance with the Declaration of Helsinki. Briefly, PBMCs were obtained by gradient centrifugation with Ficoll (GE Healtchcare, Chicago, USA), washed twice and immediately processed for monocyte isolation. Monocytes were isolated by positive selection using $CD14^+$ MicroBeads UltraPure, human (Miltenyi Biotec, Bergisch Gladbach, Germany). After isolation, monocytes were counted and cultured at 1×10^6 cell/mL in CellGro GMP DC medium (CellGenix, Freiburg, Germany) complemented with 2% human serum ((Biowest, Nuaillé, France), IL-4 (250 IU/mL) and GM-CSF (500 IU/mL) (Miltenyi Biotec, Bergisch Gladbach, Germany) at 37 °C. On Day 2, cells are replenished with fresh medium and cytokines. On Day 4, immature cells are harvested by gently tapping the flask and HOCl-oxidized Me290 lysate was added to moDCs at a cell ratio of 1:1 for 24 h. On Day 5, cells were matured for 16 h in the presence of IFNγ (2000 IU/mL, Miltenyi Biotec, Bergisch Gladbach, Germany) and lipopolysaccharide (LPS, 60 EU/mL, Sigma, Darmstadt, Germany). Matured cells were finally harvested and cryopreserved at $5–10 \times 10^6$ cells/mL in 90% human serum (Biowest, Nuaillé, France), 10% DMSO (AppliChem, Darmstadt, Germany) and stored in liquid nitrogen until further use.

2.3. In vitro stimulation (IVS)

To characterize PBMCs stimulated with HOCl-loaded moDCs, three rounds of *ivs* were performed. MoDCs were thawed and resuspended at 0.5×10^6 cells/mL in RPMI supplemented with 8% Human AB serum, 5% Penicillin-Streptomycin, 5% sodium pyruvate, 5% Non Essential Amino Acids, 5% Kanamycin, 0.5% 2-beta mercaptoethanol 50 mM (Gibco by Life Technologies, Grand Island, NY, USA) (R8 medium). Cells were plated in a 48 well plate. Autologous PBMCs were thawed and resuspended at 0.5×10^6/mL in R8 medium supplemented with 50 U/mL IL-2 (PreproTech, Rocky Hill, NJ, USA) and plated at a DC:T cell ratio 1:10 and incubated at 37 °C 5% CO_2. On Day 2, cells were replenished with fresh medium with IL-2 in the presence of the desired modulators: IL-12 at 10 ng/mL, 4-1BBL at 5 μg/mL (PeproTech, Rocky Hill, NJ, USA), IL-18 at 100 ng/mL (Bio-Techne, Minneapolis, MN, USA), IL-21 at 100 ng/mL, IL-15 at 50 ng/mL, IFNγ at 5 ng/mL, CD40L at 5 μg/mL (Miltenyi Biotec, Bergisch Gladbach, Germany), anti-CTLA-4 and anti-PD-L1 at 10 μg/mL (Thermo Fisher Scientific, Massachusetts, USA). Every 2–3 days cells were replenished with fresh medium with the desired modulators. On Day 7, PBMCs were stimulated for another round with thawed antigen-loaded DCs at the same DC:T cell ratio of 1:10 and with compound additions, as indicated above. The stimulation was repeated for a total of three rounds, at the end of the stimulation cells were harvested and analyzed with the assays reported below.

2.4. Tetramer and phenotype staining

Stimulated PBMCs were stained with MART-1 Tetramer (TCMetrix, Lausanne, Switzerland) PE, anti-CD3 PE/Dazzle 594, anti-CD8 AF700, anti-CD45RA FITC, anti-CD4 PerCP/Cy5.5, anti-CD25 BV605, anti-CD127 APC/Cy7, anti-CD39 APC, anti-CD73 PE/Cy7 (all antibodies from Biolegend, San Diego, CA, USA). Dead cells were excluded using Zombie Aqua (Biolegend, San Diego, CA, USA). Briefly, cells were resuspended and washed in PBS supplemented with 2% FBS (Gibco by Life Technologies, Grand Island, NY, USA), incubated for 45 min at room temperature in the presence of MART-1 tetramer, washed twice and incubated with the indicated antibodies for 20 min at 4 °C, cells were finally washed and analyzed by flow cytometry with a Fortessa instrument (BD Biosciences, San Jose, CA, USA).

2.5. Cytokine production assay

Stimulated PBMCs were incubated with Me290 tumor cells at a tumor cell:PBMCs ratio of 1:10 for 2 h at 37 °C. Brefeldin A (Biolegend, San Diego, CA, USA) was added in the well at 5 ng/mL and incubated for an additional 3 h at 37 °C. The cells were then washed and stained with the following antibodies: anti-CD3 PE/Dazzle 594, anti-CD8 AF700, anti-CD56 BV421, anti-CD16 PE, anti-CD4 PerCP/Cy5.5 (Biolegend, San Diego, CA, USA) for 20 min at 4 °C. Cells were then washed, fixed and permeabilized using the Cyto-Fast™ Fix/Perm Buffer Set (Biolegend, San Diego, CA, USA) according to manufacturer instructions and subsequently

intracellularly stained with the following antibodies: anti-IFNγ AF647, anti-TNFα FITC and anti-IL2 PE/Cy7 (Biolegend, San Diego, CA, USA) for 20 min at 4 °C. Samples were then analyzed by flow cytometry with a Fortessa instrument.

2.6. Tumor killing assay

To assess tumor killing activity, stimulated PBMCs were incubated with Me290 tumor cells at a 1:5 target:effector cells cell ratio, in the presence of a green caspase-3/7 reagent (Essen Bioscience. Ann Arbor, MI, USA). Cells were then imaged every 2 h with the IncuCyte Instrument (Essen Bioscience. Ann Arbor, MI, USA). Total green area/mm^2 was then calculated using the IncuCyte Zoom software (Essen Bioscience, Ann Arbor, MI, USA) to estimate tumor cell death. Three technical replicates were used for the tumor killing assay.

2.7. Natural Killer (NK) functional assay

Stimulated PBMCs were rested in RPMI medium supplemented with 10% FBS in the presence of 50 U/mL IL-2 (Peprotech, Rocky Hill, NJ, USA) and 5 ng/mL IL-15 (Miltenyi Biotec, Bergisch Gladbach, Germany) for 8–9 h. Cells were then incubated with K562 cells (kind gift of Dr Selena Vigano, University of Lausanne, Switzerland) at a 1:2 cell ratio in the presence of Brefeldin A (Biolegend, San Diego, CA, USA) and anti-CD107 BV510 (BD) overnight. The next day, cells were harvested and stained with anti-CD3 BV605, anti-CD56 PE, anti-CD16 AF700, anti-NKp46 Pe/Cy7 (Biolegend, San Diego, CA, USA), and viability dye Zombie IR (Biolegend, San Diego, CA, USA) for 20 min at 4 °C. Cells were then fixed and permeabilized using the Cyto-Fast™ Fix/Perm Buffer Set (Biolegend, San Diego, CA, USA). Intracellular staining was performed by incubating cells with anti-IFNγ APC and anti-TNFα FITC (Biolegend, San Diego, CA, USA) for 20 min at 4 °C. Sample were then analyzed by flow cytometry using the Fortessa instrument.

2.8. Bioinformatic analysis

2.8.1. Data preprocessing

Subtracting the baseline. For each treatment (either single or double) the values obtained at the condition with only IL-2 (baseline) were subtracted, so that the resulting numerical values are relative to this condition. Hence, these values can be either positive or negative for values higher and lower than the baseline, respectively.

Normalization of all readouts to range between 0 and 1. After subtracting the baseline, the data matrix was transformed in order to harmonize the dynamic range, so that those features with a greater dynamic range do not weigh more than the others by nature. For this purpose, the data was transformed as follows:

$$y_i = \frac{x_i - \min(x)}{\max(x) - \min(x)}$$

where x is a set including all the values across samples and conditions for a given functional/phenotypic feature, and $x_i$and y_i corresponds to the untransformed and transformed values, respectively, for feature i.

Missing data in the resulting matrix was imputed by adopting, for each feature, the average value across all samples and conditions (treatments) for that feature, so that the imputed data have a neutral effect on the final ranking of treatments.

2.8.2. Construction of the single treatments network

The single treatments network is a bipartite graph with edges connecting two different and mutually excluding subsets of nodes: single treatments (n = 9) and features (n = 18). Within this network edges represent an impact of the treatment on the feature that is as least equal the percentile 60 of the distribution of such a feature across all samples and conditions. By doing so, we filter out the weakest effects and focus on the greatest and arguably most reliable changes. This arbitrary threshold of 60% was determined by a preliminary analysis using different thresholds to generate the Booleanized network and the comparison (correlation) of the resulting single treatment ranking with respect the ranking obtained without the Booleanization, i. e., using the numerical value of the readout (normalized to range between 0 and 1) instead of either 0 or 1 for edges present and absent, respectively (see the corresponding methods section). The correlation between the two rankings exhibited a maximum at R = 0.89 (both Pearson and Spearman) for a threshold of 60%.

2.8.3. Construction of the double treatments network

The double treatments network is a bipartite graph derived from the single treatment networks where the two disjoint subsets of nodes are double treatments (n = 36) and functional/phenotypic features (n = 18). Within this network edges connecting double treatments and features are present if, and only if, at least one of the constituent elements of the combination was connected to the features within the single treatments network.

2.8.4. Scoring combinations

The score for a given treatment (either double or single) is calculated as follows:

$$Score = \sum feature_i \times weight_i$$

where $feature_i$ takes values of 0 and 1 if the link is absent or present within the corresponding network (either single or double treatment network).

3. Results

3.1. A screening pipeline to assess the immunogenicity of immunomodulators in combination with a DC-based vaccine

In order to predict the immunogenicity of dual combinations of immunomodulatory agents we first developed an *in vitro* system to assess the performance of a DC vaccine in the presence of immunomodulatory agents introduced as single adjuvants during the T cell priming phase. We then characterized both crucial phenotypic and functional aspects of the so-elicited immune response. Finally, we developed an algorithm to predict the immunogenicity of dual combinations, based on the experimental data of its single components (Fig. 1). In particular, for the *in vitro* screening system, human moDCs were pulsed with an oxidized lysate of the melanoma cancer cell line Me290 and matured with IFNγ and LPS, as previously described by our group [36]. Antigen-loaded and matured moDCs were then used to prime autologous PBMCs for a total of three rounds of stimulation, in the presence of the selected modulators, added as single agents. Of note, due to the essential role of IL-2 in T cell proliferation and survival [37], we always included IL-2 in all tested conditions and therefore considered it as our baseline.

Most of the selected modulators have been already investigated with DC vaccines demonstrating a good performance, when combined as single adjuvants [22,38–41]. However, the possibility of additive or synergistic effects when used in combination has mostly remained unexplored or not systematically investigated.

After the priming phase, to assess different aspects of an immune response we have selected 18 different phenotypical and functional readouts (Table 2). Each of these readouts focuses

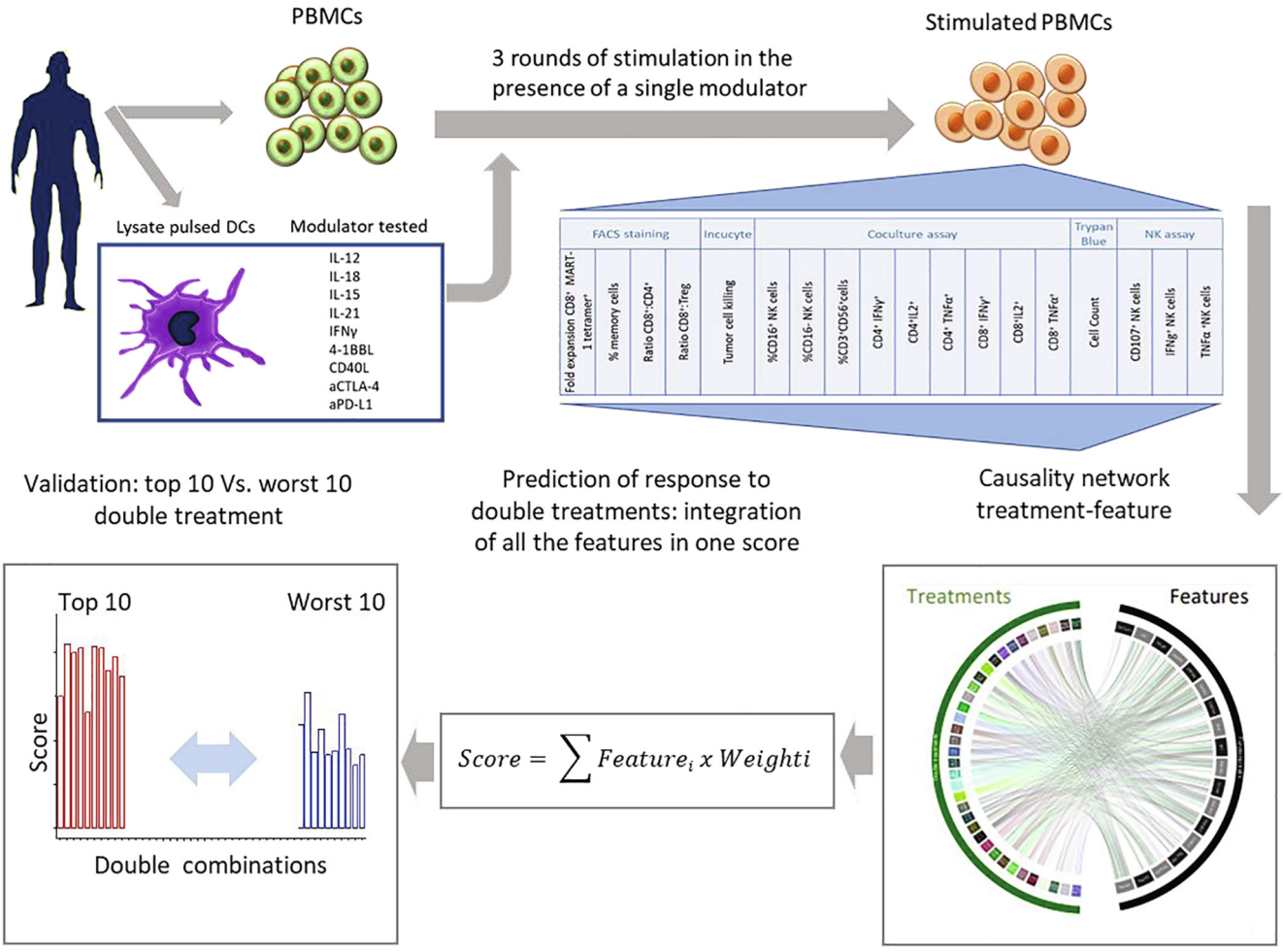

Fig. 1. Schematic diagram of the workflow for prediction of the best dual combination based on a single treatment screening. DCs are generated from monocytes isolated from the peripheral blood of healthy donors. DCs are pulsed with HOCl-oxidized tumor lysate to stimulate autologous PBMCs for a total of three rounds of stimulation. The desired modulators are individually added in the culture medium and replenished every 2–3 days. After three weeks of stimulation, stimulated PBMCs are harvested and processed into different experiments (staining, cytotoxicity assay, tumor co-culture and NK cell assay). 18 functional and phenotypical readouts are extracted to characterize the induced immune response. The different traits to the response of single treatment are then used to construct a causality network and linearly combined into a score to predict and rank the outcome of dual combinations. To assess the reliability of predictions derived from our experimental/computational platform we experimentally validated the top 10 predicted combinations and compared with respect to the 10 worst predicted treatments.

Table 2
List of selected functional and phenotypical readouts with their attributed weights. The weights were attributed based on their relative importance in the immune response.

Phenotypical and functional traits	Weight
Fold expansion of MART-1 $CD8^+$ Tetramer positive cells	5
% Effector and Central Memory in $CD8^+$ T cells	1
Ratio $CD8^+/CD4^+$	3
Ratio $CD8^+$/Treg	3
Tumor killing	5
%$CD16^+$ NK cells	2
%$CD16^-$ NK cells	2
%NKT cells	2
%$CD4^+$ IFNγ+	5
%$CD4^+$ IL-2+	5
%$CD4^+$ TNFα+	5
%$CD8^+$ IFNγ+	5
%$CD8^+$ IL-2+	5
%$CD8^+$ TNFα+	5
%$CD107^+$ NK cells	3
%$IFN\gamma^+$ NK cells	3
%$TNF\alpha^+$ NK cells	3
Cell Count	1

on different crucial features of the immune response, allowing a global view of the effects induced by the adjuvants. In particular, these include: a phenotypical analysis by flow cytometry of both $CD8^+$ and $CD4^+$ T cell compartments, the occurrence of Tregs, $CD16^+$ and $CD16^-$ NK cells and Natural Killer T cells (NKT) (Fig. S2). From a functional point of view, we evaluated the expansion of antigen-specific T cells against the MART-1 epitope expressed by Me290, by tetramer staining followed by flow cytometry analysis (Fig. S1). We also evaluated the killing capacity of stimulated PBMCs in an image-based tumor killing assay (IncuCyte assay), using Me290 as target cells. We also assessed IFNγ, TNFα and IL-2 cytokine release after co-culture of the stimulated PBMCs with the tumor cell line, by both $CD4^+$ and $CD8^+$ T cell compartments (Fig. S2). Finally, the functionality of NK cells was assessed by their degranulation and production of IFNγ and TNFα upon co-culture with K562 (Fig. S3) (Tables S1–S3).

All these different aspects are important and complementary in the induction of a potent immune response. In order to compare the performance of different combinations, we merged the different readouts in a single score. However, given the fact that not all the considered features play equal roles and contributions to the final tumor protective effect we introduced a weight system

in an attempt to reflect their relative importance. To this aim a weight spanning from 1 (lowest contribution) to 5 (higher contribution) was attributed to every readout. To attribute weights we followed the following rationale: we gave a higher priority and hence a higher weight to functional and tumor specific assays that would reflect the direct tumor killing properties elicited by the vaccine (e.g. tetramer positive $CD8^+$ T cells [55,56], tumor killing assay); we gave lower weight to phenotypic assays that reflect the activation status of immune cells but that do not necessarily reflect tumor responsiveness. In other words, the attributed weights reflect the importance of each single aspect sampled by the considered assay in contributing to tumor killing capabilities induced by the vaccine. A relative weight scale was set giving the highest score of 5 to T cell related readouts (Tetramer positive $CD8^+$ T cells, cytokine secretion by $CD4^+$ and $CD8^+$ T cells) considered as the most important players in the immune response. This was followed by the phenotypic characterization of T cells ($CD8^+$ T cell expansion, presence of Treg [59,60]) which, although important, is not directly related to the killing capacity and was therefore attributed a lower weight of 3. NK cell activation plays a role in tumor killing and eradication [61,62] although this innate immune system mechanism is less efficient and less specific than adaptive cytotoxic responses ($CD8^+$ T cells) [64] and was therefore given a weight of 3. As highlighted above, phenotypical characterization of NK cells ($CD16^+$, $CD16^-$ and NKT cells) [63] was given a lower weight of 2. The weight of 1 was attributed to the cell count at the end of the third stimulation and to the $CD8^+$ T cells memory phenotype [57,58] (A detailed explanation is provided in the supplementary) (Table 2). To calculate the score, for each readout we multiplied the experimentally obtained value by the attributed weight of that particular readout, we repeated this approach for all readouts and summed the results. The score was then used to rank the different possible dual combinations (36 combinations in total) (Table S4) out of the 9 single treatments (Fig. 1).

3.2. Prediction based on single treatments

In order to predict the outcome of a dual combinations, we first ran the *in vitro* screening as described above, with moDCs and PBMCs obtained from three different healthy donors, in the presence of the 9 different single stimuli selected in Table 1 and in the presence of IL-2 as baseline (Tables S1–S3). For every donor, experimental data obtained with single components were then used to construct a bipartite graph, named, from now on as "the single treatments network". To this aim, a donor-specific reference graph was created (Fig. 2) and a threshold at 0.6 percentile was set afterwards for each readout (see methods) in order to determine whether a single treatment can or cannot activate the corresponding readout while filtering out the weakest effects. The resulting Booleanized version of the reference graph (Fig. 3) becomes the single treatments network. It is worth noting here that the 3 networks generated on 3 different donors separately exhibited a good accordance.

A double treatment network (Fig. 3) was derived then from the single treatments network by applying the following rule: if at least one of the constituent modulators of a given combination activates the readout the dual combination inherits the link. For every donor, a score reflecting the immunogenicity of dual combinations (36 in total) was predicted using their respective double treatments network. This score is calculated as the sum of the product of the status of the feature (either 0 or 1 for absent and present links, respectively, within the double treatments network) and the corresponding weights. The score is then used to rank the dual combination from the highest to the lowest (Fig. 3).

The calculation of the predicted score was performed separately on 3 donors. The ranking of the conditions was then obtained based on the combined score of the individual scores calculated as illustrated in Table 3. It is interesting to note that most of the top predicted conditions are combined with CD40L, which is also expected to perform well as a single agent. Moreover IL-12 alone is also expected to increase the immunogenicity of the response when combined to DC vaccination.

3.3. Agreement between prediction and validation and comparison top vs bottom

To evaluate if the predicted ranking is actually discriminating between the best and the worst performers, we carried out the same functional and phenotypic assessment used for the single treatment screening on a selection of combinations, using samples from the same 3 donors. More specifically, we selected the best 10 and worst 10 combinations across the 3 donors (in red and blue, respectively, in Fig. 4), in order to compare the two groups. Fig. 4-A-B shows a bar plot of the 36 combinations of 9 single treatments ranked by their predicted response to treatment, where Fig. 4A corresponds to predicted scores, whereas Fig. 4B corresponds to scores calculated based on the validation experiments. The results of this analysis showed that the general trend of the ranking is preserved, and the best predicted combinations performed collectively better than the worst. Fig. 4C shows a boxplot representation of the two groups, with a very little overlap and the p value resulting from a T-test comparing the two groups, which was significant for an alpha of 1%. It is worth noting here that some combinations, such as CD40L+IL-15 and CD40L+IL-21, were over-estimated by our predictions (See Fig. 4B), and that the relative positions in the ranking within both tails of the score distribution for some combinations can be wrong; e.g., IL-15+IL-21 is outperformed by 4-1BBL+IL-15 (See Fig. 4B, blue tail). However, it is important to keep in mind that the intended purpose of this methodology is not to pinpoint one single combination, but to prioritize in an educated manner an affordable subset of combinations for further investigation. We have noticed a general over-estimation of the observed score in the validation dataset with respect to the predictions. This general over-estimation reflects the underlying assumption adopted by the algorithm: if two single treatments improve one distinct feature each, together they improve both features. In addition, the assumption may also lead to the misevaluation of cases were the improvement of the combination with respect to its constituent elements is based on features that are mutually excluding. However, Fig. 4 shows that, in general, the derived ranking is not affected by the skewness of the predicted score distribution and, therefore, the methodology serves to its intended purpose of prioritizing subsets of promising combinations.

Taken collectively, these observations confirmed the ability of our experimental and computational platform to predict the immunogenicity enhancement of dual combinations, based on experimental data obtained from their single components.

4. Discussion

Despite encouraging preclinical and clinical responses, DC-based vaccines still present only a modest clinical outcome. The limited performance can be explained by several mechanisms such as intrinsic factors related to patients (age, prior treatments, genetics...), the source of DCs, vaccination schedule, route of administration or different protocols used to generate vaccines [33,42]. A crucial aspect is constituted by DC's phenotype and their ability to both induce a fully developed immune response (e.g. efficient maturation, migration, signal 1, 2 and 3 signaling) and to overcome immunosuppressive mechanisms present in the tumor microenvironment. However, the immune response is a complex process as

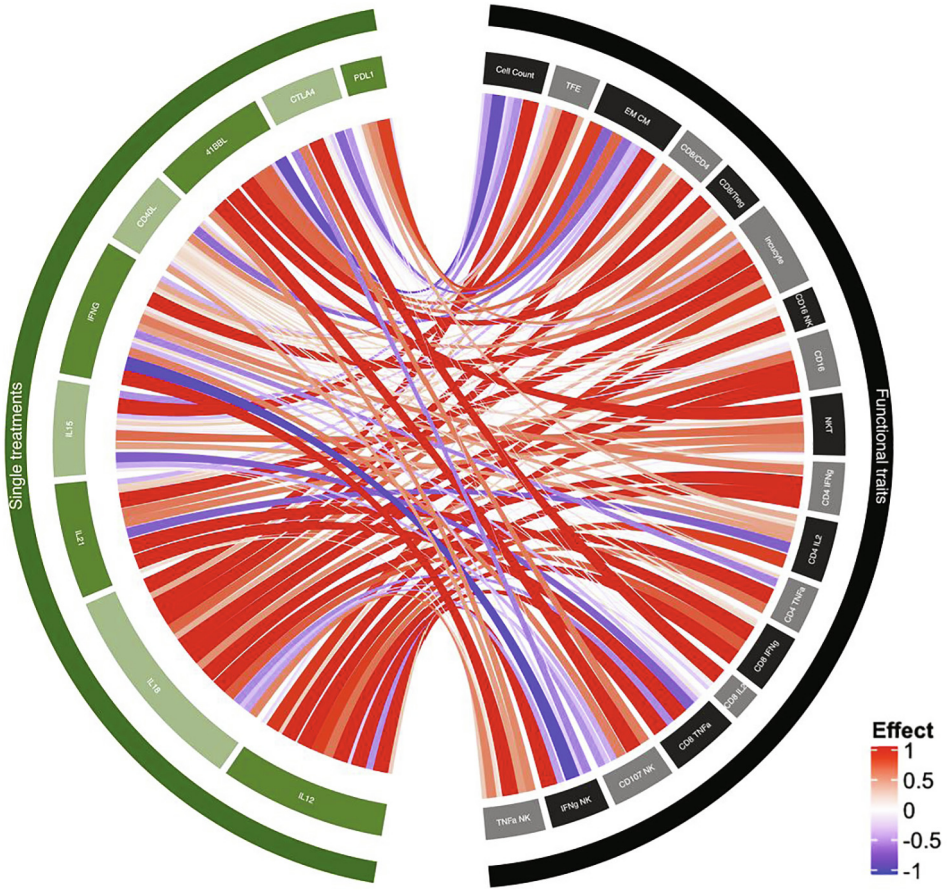

Fig. 2. Effect of single treatments on a collection of functional and phenotypical features. The chord diagram represents a reference bipartite graph connecting single treatments and functional/phenotypic features based on experimental observations. The data for each feature has been normalized and scaled for display, so that the intensity of the colors can be compared between different features. The treatment with IL-2 alone (not shown) was considered the baseline and subtracted from all readouts; consequently, the effect of a given treatment over a given feature can be either negative or positive according to their relative value with respect to the baseline (colored in blue and red, respectively). (For interpretation of the references to colour in this figure legend, the reader is referred to the web version of this article.)

both synergistic and antagonistic interplay can occur within the same response depending on the presence and dose of immunomodulators available in the environment. Therefore, combinatorial treatments targeting different aspects of the phenotype and functionality of DCs can be beneficial and potentially helpful to reach a better clinical outcome than single agents. With the very large arsenal of modulators currently available, the combinatorial problem becomes rapidly unaffordable for an exhaustive investigation; and predictive tools to prioritize and guide the experimental design become of paramount importance to accelerate DC vaccination's research and its translational applications to the clinic.

To address this challenge, we developed an experimental and computational framework, which takes the experimental data obtained with single adjuvants as the input and predicts the relative immunogenicity enhancement by dual adjuvant combinations. By doing so, a given list of combinations can be ranked by priority, so that some can be either prioritized or discarded for further investigation. In order to consider the complexity of the immune system we carefully selected 18 functional and phenotypical readouts that reflect both the T cell and NK cell induced characteristics. These readouts were combined in the calculation of a score integrating different aspects important in the generation of an immune response. Based on this score we developed a bioinformatics algorithm able to predict the immunogenicity of dual combinations of the single agents considered. It is worth noting here that despite that the algorithm does not explicitly model synergy, antagonism or additivity of the underlying mechanisms, it manages to approximate the actual immune response by integration (linear combination) of the above-mentioned parameters evaluated separately with enough precision to rank and directly compare different combinations. Indeed, after experimentally testing a selected subset of combinations in the same *in vitro* system, we observed a strong correlation between predicted and experimental results and ranking, and a clear and statistically significant separation between combinations predicted as the best and the worst.

Our study pointed out the important role of CD40L and IL-12 that were able to enhance diverse immune functions. Interestingly, these two compounds have already been used in the clinic with discreet success [38–40,43–45]. Hence, these observations confirmed the validity of the prediction tool we developed. However, we also observed for combinations of those agents and others subtle differences across the donors; future work would lead us to the exploration of greater cohorts to characterize and stratify the general human population.

Among the several immunomodulatory agents, the CD40-CD40L interaction is so far one of the most studied in DC vaccination [46–48]. This interaction between the CD40 receptor present at the surface of DCs and cognate ligand (CD40L) expressed by $CD4^+$ T cells is essential to subsequently license and activate DCs to efficiently stimulate cytotoxic $CD8^+$ T cells.

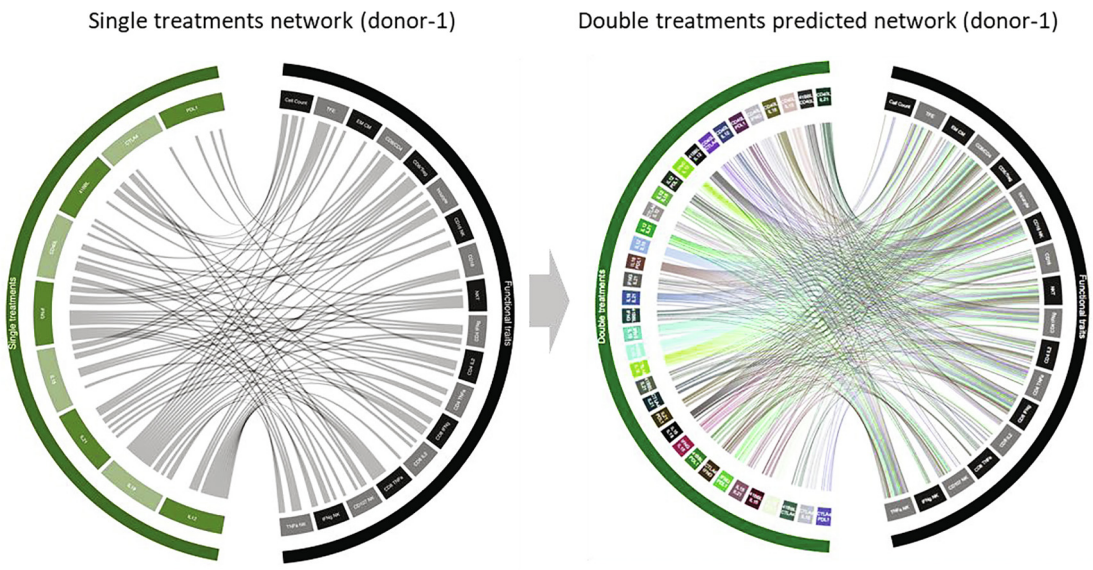

Predicted ranking of double treatments

Treatment	Score	Treatment	Score
CD40L & IL21	62	CTLA4 & IL18	50
IL12 & PDL1	61	IL21 & PDL1	48
IL12	61	IL15 & IL18	47
41BBL& CD40L	59	41BBL & IL21	46
CD40L & IFNG	59	IFNG	46
41BBL & IL12	58	41BBL & IFNG	45
IFNG & IL12	58	CTLA4 & IFNG	45
CD40L & IL18	57	IFNG & PDL1	45
CD40L & IL2	57	IL21	43
IL12 & IL21	57	CTLA4 & IL21	42
CD40L & PDL1	56	IL15& IL21	42
CD40L & IL12	56	IFNG & IL15	40
CD40L & IL15	55	41BBL & PDL1	35
CD40L & CTLA4	55	41BBL & IL15	35
IL12 & IL18	55	IL15	33
IL18 & PDL1	55	IL15 & PDL1	32
IL12 & IL15	54	41BBL	31
IL18 & IL21	53	CTLA4 & PDL1	30
CTLA4 & IL12	52	PDL1	28
IFNG & IL21	51	CTLA4 & IL2	26
IL18	50	CTLA4 & IL15	26
IFNG & IL18	50	41BBL & CTLA4	25
41BBL & IL18	50		

Calculating double treatment scores

$$Score = \sum Feature_i \; x \; Weighti$$

For a given double treatment and donor, if there is a link to $Feature_i$, $Feature_i$ = 1.
$Feature_i$ = 0, otherwise

Feature	Weight	Feature	Weight	Feature	Weight
Cell Count	1	CD16 NK	2	CD8 IFNg	5
TFE	5	CD 16	2	CD8 IL2	5
EM CM	1	NKT	2	CD8 TNFa	5
CD8/CD4	3	CD4 IFNg	5	CD107 NK	3
CD8/Treg	3	CD4 IL2	5	IFNg NK	3
Incucyte	5	CD4 TNFa	5	TNFa NK	3

Fig. 3. Calculation of the predicted double treatment score. Single treatment network. The chord diagram represents a Booleanized representation of the bipartite graph connecting single treatments and functional/phenotypic features based on experimental observations (see Fig. 2); only effects higher than the percentile 60 of variation for each feature are considered. A single treatment network is generated for each donor. Double treatments network. The chord diagram represents a Booleanized representation of the bipartite graph connecting double treatments and functional/phenotypic traits derived from the single treatment network; every double treatment inherits the edges of its constituent elements as follows: a link between a double treatment and a functional feature is considered if, and only if, at least one of its constituent elements is connected to such a feature within the single treatment network. A double treatment network is generated for each donor. Calculating double treatment scores. For each double treatment. The score is calculated as the sum of the weights of all edges present in the double treatment predicted network for each donor, and averaged afterwards across donors. Predicted ranking of double treatments. Higher scores correspond to double treatments with a greater impact on the selected functional features.

In this licensing process DCs will upregulate co-stimulatory molecules and increase the production of Th1 polarizing cytokines [49–51]. One of the consequences of the licensing is the increased production of IL-12. IL-12 is a master regulator and activator of Th1 type responses, responsible for cytotoxic effects and immune-related tumor clearance. The central importance of IL-12 is also highlighted by several studies present in the literature aimed at engineered DCs with transfection to induce a sustained IL-12 production [38,39]. So far, DCs have been already modified with IL-18 [19,39], IL-15 [22], 4-1BBL [52,53] showing promising result in preclinical studies but only very few cases progressed further and entered the clinic. A complementary approach focusing on depleting DCs of inhibitory molecules using siRNA was also recently pursued in the case of CTLA-4 [54] and PD-L1 [23]. Some dual combinations have been already tested such as IL-12 and IL-18 [38]; 4-1BBL and CD40L [52]; aPD-L1 and IL-15 [23] showing overall a good response *in vitro* with an increase in tumor reactive T cells. However, as reported in our introduction, no systematic study or comparison has been conducted so far to select optimal combinations which was the main purpose of the present study.

It is now clear that immunomodulatory agents are important adjuvants that can boost the efficacy of therapeutic DC-based vaccines. However, the large plethora of currently available agents and the ones that will likely be developed in the near future makes it difficult to estimate what best adjuvant combinations would guarantee the best clinical efficacy, without very laborious and costly screening and comparative studies. Our computational prediction tool can alleviate such expensive and time-consuming screening campaigns by being

Table 3
Ranking generated based on the combined score obtained on 3 healthy donors.

	Donor 1	Donor 3	Donor 4	Average Score
CD40L+IL21	62	60	63	61.67
IL12	61	58	61	60
41BBL+CD40L	59	59	62	60
CD40L	57	57	60	58
CD40L+IL15	55	59	60	58
CD40L+IL18	57	60	56	57.67
CD40L+IFNG	59	53	60	57.33
CD40L+aPDL1	56	59	57	57.33
CD40L+IL12	56	56	59	57
CD40L+aCTLA4	55	59	56	56.67
41BBL+IL12	58	54	57	56.33
IFNG+IL12	58	45	61	54.67
IL12+aPDL1	61	48	53	54
IL12+IL15	54	50	55	53
aCTLA4+IL12	52	53	54	53
IL12+IL21	57	49	51	52.33
IL12+IL18	55	50	46	50.33
IL18	50	40	47	45.67
IL18+aPDL1	55	32	48	45
IFNG+IL21	51	26	58	45
IL18+IL21	53	32	48	44.33
41BBL+IFNG	45	34	53	44
IFNG+IL18	50	32	49	43.67
41BBL+IL18	50	35	46	43.67
aCTLA4+IL18	50	37	42	43
41BBL+IL21	46	35	48	43
aCTLA4+IL21	42	31	55	42.67
IL21+aPDL1	48	26	53	42.33
IL15+IL18	47	34	45	42
IFNG	46	32	46	41.33
IFNG+IL15	40	27	56	41
41BBL+aPDL1	35	30	53	39.33
aCTLA4+IFNG	45	25	47	39
IL21	43	30	43	38.67
IFNG+aPDL1	45	20	50	38.33
IL15+IL21	42	28	43	37.67
41BBL+IL15	35	36	41	37.33
IL15+aPDL1	32	27	53	37.33
IL15	33	37	41	37
aPDL1	28	31	48	35.67
aCTLA4	26	35	45	35.33
41BBL+aCTLA4	25	34	47	35.33
41BBL	31	34	39	34.67
aCTLA4+IL15	26	32	43	33.67
aCTLA4+aPDL1	30	25	41	32

able to efficiently predict and rank the immunogenicity of different combinations based on experimental data from single agents. In particular, the versatility and modularity of this prediction tool enables the testing of larger pools of single treatments and of novel potential immunomodulatory agents, in order to continuously identify more potent combinations to be translated into the clinic. We believe that this tool can assist the development of more efficient DC-based vaccination strategies in the future.

CRediT authorship contribution statement

Rita Ahmed: Formal analysis, Investigation, Data curation, Writing - original draft, Visualization. **Isaac Crespo:** Software, Formal analysis, Writing - original draft, Visualization. **Sandra Tuyaerts:** Conceptualization, Methodology, Investigation, Writing - review & editing. **Amel Bekkar:** Methodology, Software, Formal analysis, Writing - review & editing. **Michele Graciotti:** Validation, Supervision, Writing - review & editing. **Ioannis Xenarios:** Conceptualization, Methodology, Writing - review & editing. **Lana E. Kandalaft:** Conceptualization, Methodology, Validation, Resources, Supervision, Project administration, Funding acquisition, Writing - review & editing.

Declaration of Competing Interest

The authors declare that they have no known competing financial interests or personal relationships that could have appeared to influence the work reported in this paper.

Acknowledgements

The authors would like to thank The Ludwig Institute for Cancer Research for its financial support. This work was supported by funding from the Anticancer Fund and Ovacure. Sandra Tuyaerts was financially supported by the Anticancer Fund and received a travel grant from the Research Fund Flanders (FWO). We would like to thank Dr Caroline Boudousquié for her precious help to set up the experiments.

Appendix A. Supplementary data

Supplementary data to this article can be found online at https://doi.org/10.1016/j.csbj.2020.08.001.

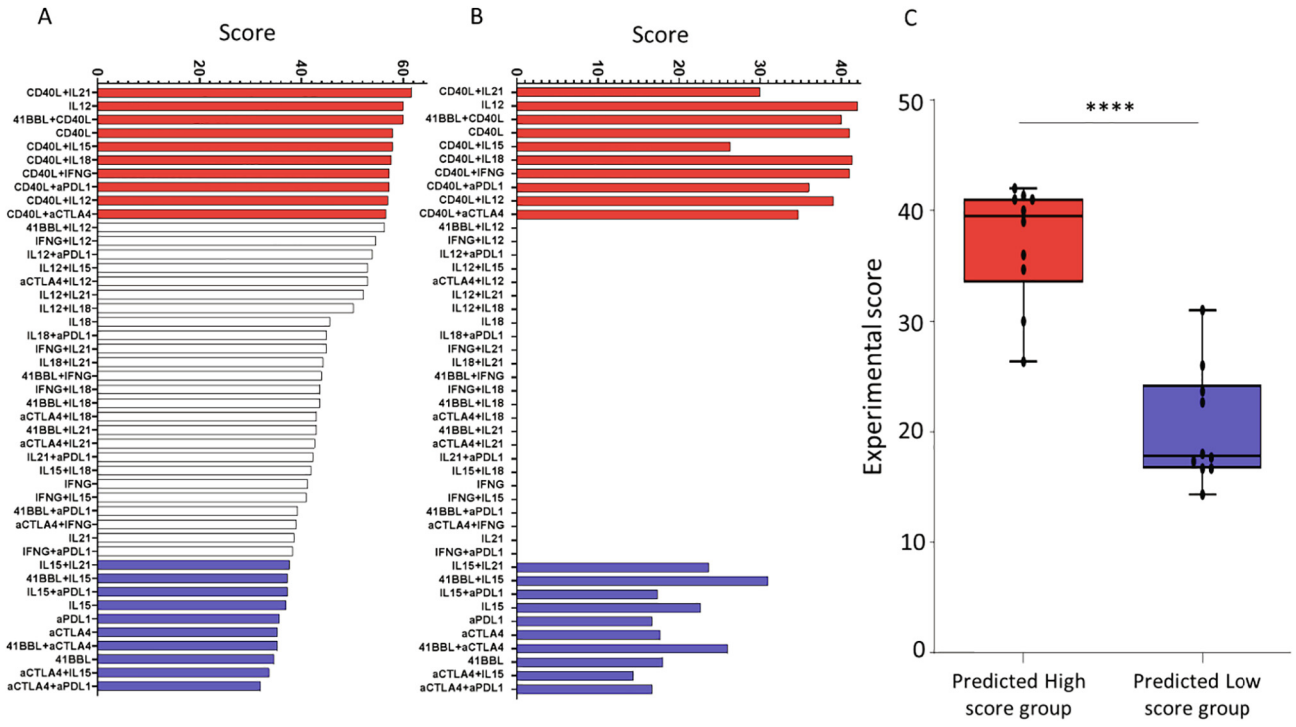

Fig. 4. Comparing the score of predictions Vs. validations. A) Predictions; bar plot representing double treatments ranked by their predicted score. The two tails of the distribution (ten best and ten worst double treatments in red and blue, respectively) were selected to carry out the corresponding validation experiments. B) Validation; bar plot representing double treatment experimental scores ordered by their predicted score. Results showed that, collectively, the best predicted treatments outperformed the worst ones. C) Boxplot comparing the scores of the best Vs. the worst treatments. The T-test exhibited a significant p-value of 1.2e-05. (For interpretation of the references to colour in this figure legend, the reader is referred to the web version of this article.)

References

[1] Bray F, Ferlay J, Soerjomataram I, Siegel RL, Torre LA, Jemal A. Global cancer statistics 2018: GLOBOCAN estimates of incidence and mortality worldwide for 36 cancers in 185 countries. CA Cancer J Clin 2018;68:394–424.

[2] Steinman RM, Cohn ZA. (1973). Identification of a novel cell type in peripheral lymphoid organs of mice. I. Morphology, quantitation, tissue distribution. J Exp Med 137, 1142-1162.

[3] Steinman RM, Witmer MD. Lymphoid dendritic cells are potent stimulators of the primary mixed leukocyte reaction in mice. Proc Natl Acad Sci 1978;75:5132–6.

[4] Banchereau J, Briere F, Caux C, Davoust J, Lebecque S, Liu Y-J, et al. Immunobiology of dendritic cells. Annu Rev Immunol 2000;18:767–811.

[5] Small EJ, Schellhammer PF, Higano CS, Redfern CH, Nemunaitis JJ, Valone FH, et al. Placebo-controlled phase III trial of immunologic therapy with sipuleucel-T (APC8015) in patients with metastatic, asymptomatic hormone refractory prostate cancer. J Clin Oncol 2006;24:3089–94.

[6] Sprooten J, Ceusters J, Coosemans A, Agostinis P, De Vleeschouwer S, Zitvogel L, et al. Trial watch: dendritic cell vaccination for cancer immunotherapy. OncoImmunology 2019;8:1638212.

[7] Zhang Z, Liu S, Zhang B, Qiao L, Zhang Y, Zhang Y. T cell dysfunction and exhaustion in cancer. Front Cell Dev Biol 2020;8:17.

[8] Veglia F, Gabrilovich DI. Dendritic cells in cancer: the role revisited. Curr Opin Immunol 2017;45:43–51.

[9] Gabrilovich DI, Ciernik IF, Carbone DP. Dendritic cells in antitumor immune responses. Cell Immunol 1996;170:101–10.

[10] Bella SD, Gennaro M, Vaccari M, Ferraris C, Nicola S, Riva A, et al. Altered maturation of peripheral blood dendritic cells in patients with breast cancer. Br J Cancer 2003;89:1463–72.

[11] Troy AJ, Summers KL, Davidson PJ, Atkinson CH, Hart DN. Minimal recruitment and activation of dendritic cells within renal cell carcinoma. Clin Cancer Res 1998;4:585–93.

[12] Brown RD, Pope B, Murray A, Esdale W, Sze DM, Gibson J, et al. Dendritic cells from patients with myeloma are numerically normal but functionally defective as they fail to up-regulate CD80 (B7–1) expression after huCD40LT stimulation because of inhibition by transforming growth factor-beta1 and interleukin-10. Blood 2001;98:2992–8.

[13] Patente TA, Pinho MP, Oliveira AA, Evangelista GCM, Bergami-Santos PC, Barbuto JAM. Human dendritic cells: their heterogeneity and clinical application potential in cancer immunotherapy. Front Immunol 2019;9:3176.

[14] Wculek SK, Cueto FJ, Mujal AM, Melero I, Krummel MF, Sancho D. Dendritic cells in cancer immunology and immunotherapy. Nat Rev Immunol 2020;20:7–24.

[15] Seder RA, Paul WE. Acquisition of lymphokine-producing phenotype by CD4+ T cells. Annu Rev Immunol 1994;12:635–73.

[16] Heufler C, Koch F, Stanzl U, Topar G, Wysocka M, Trinchieri G, et al. Interleukin-12 is produced by dendritic cells and mediates T helper 1 development as well as interferon-gamma production by T helper 1 cells. Eur J Immunol 1996;26:659–68.

[17] Grohmann U, Belladonna ML, Bianchi R, Orabona C, Ayroldi E, Fioretti MC, et al. IL-12 acts directly on DC to promote nuclear localization of NF-kappaB and primes DC for IL-12 production. Immunity 1998;9:315–23.

[18] Micallef MJ, Ohtsuki T, Kohno K, Tanabe F, Ushio S, Namba M, et al. Interferon-gamma-inducing factor enhances T helper 1 cytokine production by stimulated human T cells: synergism with interleukin-12 for interferon-gamma production. Eur J Immunol 1996;26:1647–51.

[19] Tatsumi T, Gambotto A, Robbins PD, Storkus WJ. Interleukin 18 gene transfer expands the repertoire of antitumor Th1-type immunity elicited by dendritic cell-based vaccines in association with enhanced therapeutic efficacy. Cancer Res 2002;62:5853–8.

[20] Wei L, Laurence A, Elias KM, O'Shea JJ. IL-21 is produced by Th17 cells and drives IL-17 production in a STAT3-dependent manner. J Biol Chem 2007;282:34605–10.

[21] Turksma AW, Bontkes HJ, Ruizendaal JJ, van den Heuvel H, Scholten KBJ, Santegoets SJAM, et al. Increased cytotoxic capacity of tumor antigen specific human T cells after in vitro stimulation with IL21 producing dendritic cells. Hum Immunol 2013;74:506–13.

[22] Van den Bergh J, Willemen Y, Lion E, Van Acker H, De Reu H, Anguille S, et al. Transpresentation of interleukin-15 by IL-15/IL-15Ralpha mRNA-engineered human dendritic cells boosts antitumoral natural killer cell activity. Oncotarget 2015;6:44123–33.

[23] Van den Bergh JMJ, Smits ELJM, Berneman ZN, Hutten TJA, De Reu H, Van Tendeloo VFI, Dolstra H, et al. Monocyte-derived dendritic cells with Silenced PD-1 ligands and transpresenting interleukin-15 stimulate strong tumor-reactive T-cell expansion. Cancer Immunol Res 2017;5:710–5.

[24] Mosca PJ, Hobeika AC, Clay TM, Nair SK, Thomas EK, Morse MA, et al. A subset of human monocyte-derived dendritic cells expresses high levels of interleukin-12 in response to combined CD40 ligand and interferon-gamma treatment. Blood 2000;96:3499–504.

[25] Manguso RT, Pope HW, Zimmer MD, Brown FD, Yates KB, Miller BC, et al. In vivo CRISPR screening identifies Ptpn2 as a cancer immunotherapy target. Nature 2017;547:413–8.

[26] Caux C, Massacrier C, Vanbervliet B, Dubois B, Van Kooten C, Durand I, Banchereau J. Activation of human dendritic cells through CD40 cross-linking. J Exp Med 1994;180:1263–72.

[27] DeBenedette MA, Shahinian A, Mak TW, Watts TH. Costimulation of CD28- T lymphocytes by 4-1BB ligand. J Immunol (Baltimore, Md: 1950) 1997;158:551–9.
[28] Goodwin RG, Din WS, Davis-Smith T, Anderson DM, Gimpel SD, Sato TA, et al. Molecular cloning of a ligand for the inducible T cell gene 4-1BB: a member of an emerging family of cytokines with homology to tumor necrosis factor. Eur J Immunol 1993;23:2631–41.
[29] Rudd CE, Taylor A, Schneider H. CD28 and CTLA-4 coreceptor expression and signal transduction. Immunol Rev 2009;229:12–26.
[30] Gonzalez H, Hagerling C, Werb Z. Roles of the immune system in cancer: from tumor initiation to metastatic progression. Genes Dev 2018;32:1267–84.
[31] Lion E, Smits ELJM, Berneman ZN, Van Tendeloo VFI. NK cells: key to success of DC-based cancer vaccines?. Oncologist 2012;17:1256–70.
[32] Zhang J, Shi Z, Xu X, Yu Z, Mi J. The influence of microenvironment on tumor immunotherapy. FEBS J 2019;286:4160–75.
[33] Martin Lluesma S, Wolfer A, Harari A, Kandalaft LE. Cancer vaccines in ovarian cancer: how can we improve?. Biomedicines 2016;4.
[34] Perez CR, De Palma M. Engineering dendritic cell vaccines to improve cancer immunotherapy. Nat Commun 2019;10.
[35] Ahmed R, Sayegh N, Graciotti M, Kandalaft LE. Electroporation as a method of choice to generate genetically modified dendritic cell cancer vaccines. Curr Opin Biotechnol 2020;65:142–55.
[36] Chiang CL, Kandalaft LE, Tanyi J, Hagemann AR, Motz GT, Svoronos N, et al. A dendritic cell vaccine pulsed with autologous hypochlorous acid-oxidized ovarian cancer lysate primes effective broad antitumor immunity: from bench to bedside. Clin Cancer Res 2013;19:4801–15.
[37] Dooms H, Kahn E, Knoechel B, Abbas AK. IL-2 induces a competitive survival advantage in T lymphocytes. J Immunol (Baltimore, Md: 1950) 2004;172:5973–9.
[38] Bontkes HJ, Kramer D, Ruizendaal JJ, Kueter EWM, van Tendeloo VFI, et al. Dendritic cells transfected with interleukin-12 and tumor-associated antigen messenger RNA induce high avidity cytotoxic T cells. Gene Ther 2007;14:366–75.
[39] Bontkes HJ, Kramer D, Ruizendaal JJ, Meijer CJLM, Hooijberg E. Tumor associated antigen and interleukin-12 mRNA transfected dendritic cells enhance effector function of natural killer cells and antigen specific T-cells. Clin Immunol 2008;127:375–84.
[40] Loskog A, Ninalga C, Tötterman TH. Dendritic cells engineered to express CD40L continuously produce IL12 and resist negative signals from Tr1/Th3 dominated tumors. Cancer Immunol Immunother 2006;55:588–97.
[41] Hobo W, Maas F, Adisty N, de Witte T, Schaap N, van der Voort R, Dolstra H. siRNA silencing of PD-L1 and PD-L2 on dendritic cells augments expansion and function of minor histocompatibility antigen-specific CD8+ T cells. Blood 2010;116:4501–11.
[42] Martin Lluesma S, Graciotti M, Chiang CL, Kandalaft LE. Does the immunocompetent status of cancer patients have an impact on therapeutic DC vaccination strategies?. Vaccines 2018;6.
[43] Kikuchi T, Moore MA, Crystal RG. Dendritic cells modified to express CD40 ligand elicit therapeutic immunity against preexisting murine tumors. Blood 2000;96:91–9.
[44] Koya RC, Kasahara N, Favaro PM, Lau R, Ta HQ, Weber JS, Stripecke R. Potent maturation of monocyte-derived dendritic cells after CD40L lentiviral gene delivery. J Immunother (Hagerstown, Md: 1997) 2003;26:451–60.
[45] Amin A, Dudek AZ, Logan TF, Lance RS, Holzbeierlein JM, Knox JJ, et al. Survival with AGS-003, an autologous dendritic cell–based immunotherapy, in combination with sunitinib in unfavorable risk patients with advanced renal cell carcinoma (RCC): phase 2 study results. J Immunother Cancer 2015;3.
[46] Calderhead DM, DeBenedette MA, Ketteringham H, Gamble AH, Horvatinovich JM, Tcherepanova IY, et al. Cytokine maturation followed by CD40L mRNA electroporation results in a clinically relevant dendritic cell product capable of inducing a potent proinflammatory CTL response. J Immunother 2008;31:731–41.
[47] Van Nuffel AM, Corthals J, Neyns B, Heirman C, Thielemans K, Bonehill A. Immunotherapy of cancer with dendritic cells loaded with tumor antigens and activated through mRNA electroporation. Methods Mol Biol (Clifton NJ) 2010;629:405–52.
[48] DeBenedette MA, Calderhead DM, Tcherepanova IY, Nicolette CA, Healey DG. Potency of mature CD40L RNA electroporated dendritic cells correlates With IL-12 secretion by tracking multifunctional CD8+/CD28+ cytotoxic T-cell responses in vitro. J Immunother 2011;34:45–57.
[49] Ma DY, Clark EA. The role of CD40 and CD154/CD40L in dendritic cells. Semin Immunol 2009;21:265–72.
[50] Elgueta R, Benson MJ, de Vries VC, Wasiuk A, Guo Y, Noelle RJ. Molecular mechanism and function of CD40/CD40L engagement in the immune system. Immunol Rev 2009;229:152–72.
[51] Ara A, Ahmed KA, Xiang J. Multiple effects of CD40-CD40L axis in immunity against infection and cancer. Immunotargets Ther 2018;7:55–61.
[52] Grünebach F, Kayser K, Weck MM, Müller MR, Appel S, Brossart P. Cotransfection of dendritic cells with RNA coding for HER-2/neu and 4-1BBL increases the induction of tumor antigen specific cytotoxic T lymphocytes. Cancer Gene Ther 2005;12:749–56.
[53] De Keersmaecker B, Heirman C, Corthals J, Empsen C, van Grunsven LA, Allard SD, et al. The combination of 4-1BBL and CD40L strongly enhances the capacity of dendritic cells to stimulate HIV-specific T cell responses. J Leukoc Biol 2011;89:989–99.
[54] Son CH, Bae JH, Shin DY, Lee HR, Choi YJ, Jo WS, et al. CTLA-4 blockade enhances antitumor immunity of intratumoral injection of immature dendritic cells into irradiated tumor in a mouse colon cancer model. J Immunother (Hagerstown, Md: 1997) 2014;37:1–7.
[55] Hanson HL, Donermeyer DL, Ikeda H, White JM, Shankaran V, Old LJ, et al. Eradication of established tumors by CD8+ T cell adoptive immunotherapy. Immunity 2000;13:265–76.
[56] Perica K, Varela JC, Oelke M, Schneck J. (2015). Adoptive T cell immunotherapy for cancer. Rambam Maimonides Med J 6, e0004-e0004.
[57] Murata K, Tsukahara T, Torigoe T. (2016). [Cancer immunotherapy and immunological memory]. Nihon Rinsho Men'eki Gakkai kaishi = Japanese journal of clinical immunology 39, 18-22.
[58] Ratajczak W, Niedźwiedzka-Rystwej P, Tokarz-Deptuła B, Deptuła W. Immunological memory cells. Cent Eur J Immunol 2018;43:194–203.
[59] Zou W. Immunosuppressive networks in the tumour environment and their therapeutic relevance. Nat Rev Cancer 2005;5:263–74.
[60] Gajewski TF, Meng Y, Blank C, Brown I, Kacha A, Kline J, Harlin H. Immune resistance orchestrated by the tumor microenvironment. Immunol Rev 2006;213:131–45.
[61] Morvan MG, Lanier LL. NK cells and cancer: you can teach innate cells new tricks. Nat Rev Cancer 2016;16:7–19.
[62] Waldhauer I, Steinle A. NK cells and cancer immunosurveillance. Oncogene 2008;27:5932–43.
[63] Bellora F, Castriconi R, Dondero A, Carrega P, Mantovani A, Ferlazzo G, et al. Human NK cells and NK receptors. Immunol Lett 2014;161:168–73.
[64] Nutt SL, Huntington ND. (2019). 17 - Cytotoxic T Lymphocytes and natural killer cells. in clinical immunology (Fifth Edition), R.R. Rich, T.A. Fleisher, W.T. Shearer, H.W. Schroeder, A.J. Frew and C.M. Weyand, eds. (London: Content Repository Only!), pp. 247-259.e241.